JNeurosci
THE JOURNAL OF NEUROSCIENCE

Research Articles: Behavioral/Cognitive

Stabilizing Immature Dendritic Spines in the Auditory Cortex: A Key Mechanism for mTORC1-mediated Enhancement of Long-term Fear Memories

https://doi.org/10.1523/JNEUROSCI.0204-23.2023

Cite as: J. Neurosci 2023; 10.1523/JNEUROSCI.0204-23.2023

Received: 2 February 2023
Revised: 30 August 2023
Accepted: 4 September 2023

Stabilizing Immature Dendritic Spines in the Auditory Cortex: A Key Mechanism for mTORC1-mediated Enhancement of Long-term Fear Memories

Giulia Concina[1*], Antonia Gurgone[1*], Elena M. Boggio[1], Alessandra Raspanti[1], Riccardo Pizzo[1], Noemi Morello[1], Enrico Castroflorio[1#], Tommaso Pizzorusso[2,3], Benedetto Sacchetti[1§], Maurizio Giustetto[1§].

[1]University of Turin, Department of Neuroscience, Corso Raffaello 30, 10125 Turin, Italy

[2]Institute of Neuroscience, National Research Council (CNR), Via Moruzzi 1, 56124 Pisa, Italy

[3]Scuola Normale Superiore. Biology laboratory BIO@SNS, Via Moruzzi 1, 56124 Pisa, Italy

[#]Present address: Institute of Photonic Sciences, Parc Mediterrani de la Tecnologia, Av. Carl Friedrich Gauss, 3, 08860 Barcelona, Spain

[*] These authors contributed equally to this work

[§]Contact Information:

Maurizio Giustetto, Department of Neuroscience, University of Turin, C.so Raffaello 30, 10125 Torino, Italy. E-mail: maurizio.giustetto@unito.it. Tel. +39-0116707725.

Benedetto Sacchetti, Department of Neuroscience, University of Turin, Corso Raffaello 30, Torino, Italy. E-mail: benedetto.sacchetti@unito.it. Tel. +39-0116708171.

Number of pages: 37
Number of figures and tables: 6
Number of words for abstract: 201
Number of words for introduction: 528
Number of words for discussion:1457

Conflicts of Interest: The authors do not have financial disclosures or conflict of interest to declare.

Fundings: This work was supported by the Grant "Progetti di ricerca di Rilevante Interesse Nazionale (PRIN)" 2017 (BS, Project n. 20178NNRCR_002) from the Italian Ministry of University and Research (MIUR), Fondazione Cariverona 2018 (BS) and Fondazione CRT (BS). PRIN2017 2017HMH8FA to TP; International Foundation for CDKL5 Research (MG 2015); Telethon Grant GGP11147 to MG and TP.

Author's contributions

GC, AG and EB designed the study with BS and MG. GC, and AG conducted behavioral tests analyses. AG performed immunohistochemical and biochemical experiments. EB and TP conducted two-photon imaging experiments. GC, AG and EB analyzed the data with AR, RP and NM. All authors contributed to the interpretation of results. MG and BS wrote the paper and all authors contributed to the final version of the manuscript.

ABSTRACT

Mammalian target of rapamycin (mTOR) pathway has emerged as a key molecular mechanism underlying memory processes. Although mTOR inhibition is known to block memory processes, it remains elusive whether and how an enhancement of mTOR signaling may improve memory processes. Here we found in male mice that the administration of VO-OHpic, an inhibitor of the phosphatase and tensin homolog (PTEN) that negatively modulates AKT-mTOR pathway, enhanced auditory fear memory for days and weeks, while it left short-term memory unchanged. Memory enhancement was associated with a long-lasting increase in immature-type dendritic spines of pyramidal neurons into the auditory cortex. The persistence of spine remodeling over time arose by the interplay between PTEN inhibition and memory processes, as VO-OHpic induced only a transient immature spines growth in the somatosensory cortex, a region not involved in long-term auditory memory. Both the potentiation of fear memories and increase in immature spines were hampered by rapamycin, a selective inhibitor of mTORC1.

These data revealed that memory can be potentiated over time by the administration of a selective PTEN inhibitor. Besides disclosing new information on the cellular mechanisms underlying long-term memory maintenance, our study provides new insights on the cellular mechanisms that aid enhancing memories over time.

Significance Statement

The neuronal mechanisms that may help improve the maintenance of long-term memories are still elusive. The inhibition of mammalian-target of rapamycin (mTOR) signaling shows that this pathway plays a crucial role in synaptic plasticity and memory formation. However, if its activation may strengthen long-term memory storage is unclear. We assessed the consequences of positive modulation of AKT-mTOR pathway obtained by VO-OHpic administration, a phosphatase and tensin homolog inhibitor, on memory retention and underlying synaptic modifications. We found

that mTOR activation greatly enhanced memory maintenance for weeks by producing a long-lasting increase of immature-type dendritic spines in pyramidal neurons of the auditory cortex. These results offer new insights on the cellular and molecular mechanisms that can aid enhancing memories over time.

Key Words: mTOR, PTEN inhibition, learning and memory, auditory cortex, dendritic spines

INTRODUCTION

mTOR and its downstream targets, including ribosomal protein S6 kinase (S6K) and eukaryotic elongation factors 1A and 2 (eEF1A and eEF2), play an important role in synaptic plasticity (Hoeffer and Klann, 2010; Graber et al., 2013; Saxton and Sabatini, 2017). These proteins are mostly involved in the mRNAs recruitment to ribosomes and regulate the initiation and elongation phases of translation (Hay and Sonenberg, 2004; Roux and Topisirovic, 2018). Moreover, S6K integrates signaling from mTOR, phosphoinositide 3-kinases (PI3K), and extracellular signal–regulated kinase (ERK) to modulate protein synthesis. This process starts with the phosphorylation of the ribosomal protein S6 (rpS6), a component of the 40S ribosome, which in turn modulates protein synthesis (Bohlen et al., 2021).

mTOR exists in two distinct complexes, mTORC1 and mTORC2 (Hay and Sonenberg, 2004). The first, which displays sensitivity to rapamycin, promotes different arrays of anabolic processes, and it is linked to both transcriptional and translational machinery. mTORC2 acts through rapamycin-insensitive mechanisms and promotes cell survival in response to growth factors stimulation and stress (Jacinto et al., 2006; Shiota et al., 2006; Zhou and Huang, 2010). The importance of mTORC1 for learning and memory was revealed by showing that rapamycin-induced inhibition of mTORC1 blocks long-term memory (Mac Callum et al., 2014; Garza-Lombò and Gonsebatt, 2016).

In accordance with these data, fear learning triggers an increase in mTORC1 activity and the phosphorylation of S6K1 in mice (Sun et al., 2016; Switon et al., 2017; Koehl et al., 2021), while mice carrying mutations of downstream targets of mTORC1 (i.e., 4E-BP2, S6K1, and S6K2) show abnormal long-term memory (Costa-Mattioli et al., 2009). Also, the mTORC2-mediated control of actin polymerization has been linked to long-term memory (Huang et al., 2013). Nevertheless, the cellular mechanisms through which mTORC1 and mTORC2 underlie memory processes are yet to be defined. Moreover, most studies have tested the effects of mTOR blockade on memory processes, while it remains largely unknown whether and how an enhancement of mTOR activity

and its downstream targets may improve memory formation. Although several inhibitors of the mTOR pathway are available, very few compounds can enhance its activity. Putative candidates have arisen by studying selective inhibitors of the phosphatase and tensin homolog deleted on chromosome 10 (PTEN), a phosphatase that dephosphorylates phosphatidylinositol (3,4,5)-trisphosphate (PIP_3) counteracting PI3K and resulting in the inhibition of AKT, an upstream positive regulator of mTOR (Rosivatz et al., 2006). The balance between PTEN and PI3K activities determines the cellular levels of PIP3, which is a critical regulator of the serine/threonine kinase AKT to link growth factor signaling with cellular metabolism and survival (Iwanami et al., 2009). Interestingly, PI3K activation was able to increase the formation of new dendritic spines in cultured hippocampal neurons and improve hippocampal-dependent learning (Enriquez-Barreto et al., 2014). Recent studies showed that the infusion of the water-soluble vanadium-based complex 3-hydroxypicolinate vanadium (VO-OHpic) in mice prevented PTEN-dependent dephosphorylation of PIP3 (Rosivatz et al., 2006; Mak et al., 2010) and rescued synaptic function and memory dysfunctions in cellular and animal models of Alzheimer's disease (Knafo et al., 2016). Here, we investigated the effects of VO-OHpic treatment in healthy mice in order to assess whether and how an enhancement of mTOR activity improves memory performance.

MATERIALS AND METHODS

Animals

All procedures were performed in accordance with the European Community Council Directive 2010/63/UE for care and use of experimental animals with protocols approved by the Italian Minister for Scientific Research (Authorization number 175/2015-PR) and the Bioethics Committee of the University of Torino, Italy. Animal suffering was minimized, as was the number of animals used. Mice were bred in the internal facility of the Dept. of Neuroscience. After weaning, mice were housed 4 per cage on a 12 h light/dark cycle (lights on at 7:00 h) in a temperature-controlled environment (21 ± 2°C) with food and water ad libitum. For this study, 8-9 weeks old male C57BL/6J mice were used. Because we did not observe any noticeable interindividual phenotypic or metabolic (e.g. weight and health condition scores) difference among the mouse cohorts used in this study, no inclusion/exclusion criteria were adopted besides age and sex (male) of the animals. Two-photon imaging was performed using 8 weeks old male mice carrying the Thy1-GFP transgene (M-line) as in (Landi et al., 2011). All analyses were conducted by investigators blinded to both
treatment and training of mice.

Drug treatments

The PTEN inhibitor, VO-OHpic, was dissolved in a saline + 10% DMSO solution (vehicle) and administered intraperitoneally (i.p.) at the dose of 10 µg/kg (Mak et al., 2010). Biochemical analyses were carried out 30 min and 6h after the injection. In behavioral studies, mice were injected intraperitoneally (i.p.) immediately after fear learning. Rapamycin was injected i.p. at the dose of 4.5 mg/kg dissolved in saline + DMSO 10%.

In a group of mice, VO-OHpic 10 µM was directly injected into the dorsal hippocampus. In this case, mice were anesthetized immediately after fear learning, placed on a stereotaxic frame, and

VO-OHpic or vehicle solution was delivered bilaterally (1 µL per side) into the dorsal hippocampus (DH, AP -2.3, L ± 1.5, and V –2.0) according to the Franklin and Paxinos atlas (Paxinos and Watson, 2007) at a rate of 0.5 µl/min. The injection needle was left in place for 1 min after infusion to allow for drug diffusion. The correct needle track was verified on Nissl-stained brain coronal sections.

Western blotting

Brain sample (excluding cerebellum and brainstem) were extracted with RIPA lysis buffer (1% Triton X-100, 150 mM sodium chloride, 50 mM Tris-HCl, pH 7.5, protease inhibitors (Roche), 1 mM phenylmethylsulfonyl fluoride, 1 mM sodium vanadate, 1 mM sodium fluoride, 1 mM DTT). Equal amounts of proteins (100 µg) were resolved by reducing SDS-PAGE and transferred to PVDF membrane (Amendola et al., 2014). Membranes were blocked in a blocking buffer consisting of 5% Bovine Serum Albumin (BSA) dissolved in TBST (Tris-buffered saline/0.1% Tween-20) for 1 h at 37°C. The primary antibodies were dissolved in TBST containing 1% BSA and the blots were incubated at 4°C overnight with constant shaking. The day after the membranes were incubated with the appropriate secondary antibodies (anti-mouse or anti-rabbit, 1:5000; Sigma, Italy) for 1h at RT. The chemiluminescent signal was visualized using ClarityTM Western ECL Blotting Substrates (Bio- Rad; Italy) and analyzed with Image J software (NIH, Usa). For the total protein recognition, the membranes incubated with the phospho-specific antibodies were stripped with stripping buffer containing 2-mercaptoethanol, 1% SDS, and 62.5 mMTris-HCL, pH 6.8 at 37°C for 30’ and reprobed with the total antibodies. The protein amount was normalized relative to the optical density of vinculin or β-actin; in the table 1 are reported the antibody used to perform the biochemical analyses.

176

177

178

179

180 **Table 1. List of antibodies used**

Primary Antibody	Species of origin	Working dilution		Supplier and catalog no.
		WB	IHC	
p-Akt^{Ser473}	Rabbit	1:1000		Cell Signaling and Technology Labs cod #9271
Akt	Rabbit	1:1000		Cell Signaling and Technology Labs cod #4691
p-rpS6$^{Ser240-4}$	Rabbit	1:1000	1:1000	Cell Signaling and Technology Labs cod #2215
rpS6	Rabbit	1:1000		Cell Signaling and Technology Labs cod #2217
p-ERK1/2$^{Thr202/Tyr204}$	Rabbit	1:1000		Cell Signaling and Technology Labs cod #4370
ERK1/2	Rabbit	1:1000		Cell Signaling and Technology Labs cod #9194
β-actin	Rabbit	1:1000		Cell Signaling and Technology Labs cod #4970
BDNF	Rabbit	1:500		Santa Cruz Biotechnology cod #sc-65514
p-TrkB^{Y816}	Rabbit	1:500		Abcam cod #ab229908
TrkB	Mouse	1:500		Santa Cruz Biotechnology cod #sc-7268
EF1α	Mouse	1:2000		Millipore cod #05-235
Vinculin	Rabbit	1:1000		Abcam cod #ab219649

181

Diolistic labeling and morphological analysis of dendritic spines

Fluorescence labeling of neuronal structures was performed as we previously described (Meziane et al., 2016). Tefzel tubing (Bio-Rad) was placed on a tubing preparation station (Bio-Rad) and filled with polyvinylpyrrolidone (0.32 mg/ml). 1,1′-dioctadecyl-3,3,3′,3′-tetramethylindocarbocyanine perchlorate crystals (DiI; Invitrogen) were dissolved in methylene chloride (Supelco) and then gently dropped onto the tungsten particles (1.3 µm in diameter; Bio-Rad). DiI-coated particles were immersed in distilled water, and the solution was vortexed, sonicated, and then immediately injected into the pre-dried tubing. Finally, the particle-coated tube was rotated and air-dried under constant nitrogen flow (0.2 l/min) for 1 hr and subsequently cut into small pieces (microcarriers) that were stored in a desiccated environment at room temperature. Mice were anesthetized and perfused with 4% PFA in 0.1 M PB. Brains were postfixed in the same fixative solution, washed several times in PB 0.1 M, and then cut into 300 µm sections on a vibratome (Leica VT 1000S). A commercially available helios gene gun system (Bio-Rad) was used to propel DiI-coated particles into fixed slices. A membrane filter with a 3.0 µm pore size (Millipore) was placed between the gun and the tissue to filter out large clusters of coated particles. The particles were accelerated with a shot of inert helium gas (200 psi), slices were then placed in 4% PFA for 2 hr, washed 3 times in PB 0.1 M, and mounted on glass slides. A confocal microscope (LSM-5 Pascal or LSM 900; Zeiss, 191 DE) equipped with a 40× oil-immersion objective was used to acquire images from fluorescently labeled secondary and tertiary branches of dendrites in the L2-3 of somatosensory (S1) and the secondary auditory cortex (Te2).

For each experimental group, at least 8 neurons per animal, for a total of 3-4 animals, were identified by using 4 coronal sections. From each section, at least 10 Z-stack images spaced 0.5 µm apart were collected to generate the data set, resulting in at least 1000 spines analyzed per group. Dendritic segments and spines size were analyzed quantitatively with ImageJ software (version 1.34S; NIH, public domain). Mean spine density was measured as the number of spines per dendritic length unit (µm), with an independent replicate (animal) used as the sampling unit. Neck-

length and head-diameter dimensions were used to calculate neck/head ratios as in (Meziane et al., 2016) to identify spine types as follows: mature spines, including mushroom (neck/head ratio < 1.1) and stubby (without a neck) protrusions; immature spine, including thin spines (neck/head ratio > 1.1) and filopodia .

Immunohistochemistry and quantitative analysis

Animals were anesthetized 30 min after vehicle/VO-OHpic treatment, transcardially perfused with 4% PFA, and brains were dissected and kept in the same fixative solution overnight at 4°C. After several washes in 0.1 M PB, the brains were then cryoprotected by immersion in 10, 20, and 30% sucrose solutions and subsequently cut into 30-µm sections with a cryostat. Free-floating immunostaining and diaminobenzidine reaction was performed as previously described (Amendola et al., 2014; Chapleau et al., 2012; Ciccarelli et al., 2013; Pizzo et al., 2016). After a blocking step in a PBS solution containing 0.05% Triton X-100 and 10% normal goat serum (NGS), sections were then incubated overnight at room temperature with rabbit anti-phospho-rpS6$^{Ser240-4}$ (Table1) diluted in PBS with 3% NGS and 0.05 Triton X-100. Sections were then washed and incubated for 1 h with goat anti-rabbit biotinylated secondary antibodies (1:250; Vector Labs, Burlingame, CA, USA) diluted in 3% NGS and 0.05% Triton X-100 in PBS and transferred to a solution containing a biotin–avidin complex (1:100, Vector Labs). The peroxidase reaction product was visualized by incubation in a solution containing 3,3′-diaminobenzidine (0.05% in Tris–HCI, pH 7.6) with 0.01% H2O2 for 3 min. Sections were mounted on gelatin-coated glass slides.

To evaluate changes of p-rpS6$^{Ser240-4}$ immuno-positive neurons, we acquired images of three non-consecutive coronal brain sections from 4-6 animals per group that included S1 or Te2 cortices according to a mouse brain atlas (Paxinos and Watson, 2007). A transmitted-light microscope (Eclipse 800, Nikon, Japan) equipped with a CCD camera (Axiocam HRc, Zeiss, Germany) with a 10x objective (1.0 NA) was used by keeping the bright-field illumination settings constant. A digital box (230.34 µm width) spanning from the pial surface to corpus callosum was superimposed

234 at matched locations on each coronal section of the cerebral cortex. Background values were
235 measured in the corpus callosum, and subtracted from each image using ImageJ software. The total
236 density of p-rpS6$^{Ser240-4}$ immunolabelled cells was manually quantified using the point tool in
237 ImageJ as in (Pizzo et al 2016).
238
239 **Behavioral procedures**
240 A Skinner box module was employed as a conditioning chamber as in previous work (Sacchetti et
241 al., 2002; Grosso et al., 2015). Lateral walls and ceiling were made of stainless steel while the rear
242 and front door were of transparent plexiglass. The floor was made of stainless-steel rods connected
243 to a shock delivery apparatus. The apparatus was enclosed within a sound-attenuating chamber.
244 Once inside, the animals were left undisturbed for 2 min. After this time, seven auditory stimuli (8
245 s, 80 dB, 1000 Hz, 22-s intertrial interval) acting as conditional stimulus (CS) were administered by
246 a loudspeaker. The last 1 s of each CS was paired with an unconditional stimulus (US) consisting of
247 a scrambled electric foot shock (intensity, 0.5 mA). Mice were left in the chamber for an additional
248 1 min, and then returned to the home cage.
249 Contextual fear memory was tested 48h after training. Mice were returned to the conditioning
250 chamber and freezing was monitored for 3 min. The mouse behavior was recorded by means of a
251 digital video camera and freezing was measured. Auditory memory retention was tested as short
252 term memory at 1 h or as long-term memory at 72h, 2 weeks and 4 weeks after training, in a totally
253 different apparatus located in a separate experimental room to avoid conditioned fear behavior to
254 contextual cues (Sacchetti et al., 1999; Sacco and Sacchetti, 2010). The apparatus was a 30 cm x 20
255 cm plastic cage with the floor and the sides walls made of transparent plastic, a grid top on the
256 ceiling and enclosed within a sound-attenuating chamber equipped with an exhaust fan, which
257 eliminated odorized air from the enclosure and provided background noise of 60 dB. Once inside,
258 the subject was left undisturbed for 2 min. After this time, seven CSs were administered identical to
259 those used during conditioning. To test the specificity of auditory memory processes, mice were

tested with a novel 15 kHz tone (8s, 75 dB, 15 kHz, 42-s intertrial interval). Freezing response, defined as the complete absence of somatic mobility except for respiratory movements, was taken as a fear index and measured by means of a stopwatch.

Two-photon in-vivo imaging

For in-vivo dendritic spines analyses, control and VO-OHpic-injected male mice were analyzed. Animals were oxygenated and kept warm during both surgery and imaging. Mice were maintained under avertin anesthesia (1ml/50mg) and a craniotomy of about 3 mm of diameter was made (Della Sala et al., 2016) over the primary somatosensory cortex (2 mm posterior from bregma, 2 mm lateral from lambda) to obtain an implanted cranial window. The apical dendrites of LV pyramidal neurons in the I – II/III cortical layers were imaged using a custom-built two-photon microscope based on a modified confocal scanhead (Olympus Fluoview) and mode-locked Ti:sapphire laser (Coherent Mira 900) equipped with a 20x water immersion microscope objective (NA = 0.95) at zoom 10 and a resolution of 1024x1024 pixels. Two imaging sessions 1 hour apart were made before the vehicle or VO-OHpic injection to obtain a baseline of spine dynamic. Then mice received an intraperitoneal injection of VO-OHpic solution or vehicle solution and were allowed to recover in their cages. After 5 hours mice were anesthetized and two further imaging sessions one hour apart of the dendritic segments previously analyzed were made. To identify the same dendritic segments throughout the whole imaging sessions, low magnification images were taken to obtain a map of the blood vessels and the dendritic organization in the area of interest.

ImageJ software was used to analyze the imaged dendrites. Twenty-five dendrites for a total of 1,36 mm of length and 31 dendrites for a total of 1,68 mm of length were considered for control and injected mice respectively. Each dendritic spine was followed through the imaging sessions and categorized as permanent if present in all the imaging sessions, gained or lost if it appears or disappears respectively during the imaging sessions. The turnover ratio was calculated as the

number of gained (Ng) or lost (Nl) spines on the total number (Nt) of spines (Ng+Nl)/2Nt. The spine gain and loss fraction were calculated as Ng/Nt and Nl/Nt respectively (Landi et al., 2011).

Statistical analysis

All data are presented as mean ± SEM. Parametric statistics were employed throughout all the experiments. Data from two groups were compared using two-tailed unpaired Student's t-tests. Multiple-group comparisons were assessed using two-way ANOVA followed by Fisher's LSD post-hoc test. Cumulative frequencies of dendritic spine neck/head ratio in treated and untreated animals were compared using the normal distribution Kolmogorov–Smirnov (KS) fitting test. The null hypothesis was rejected at the $p < 0.05$ level. All statistical analyses were performed using Prism software (Graphpad, La Jolla, CA, USA).

RESULTS

VO-OHpic activates AKT/mTOR pathway in mouse cerebral cortex

The PTEN inhibitor VO-OHpic has been described as the most potent and specific molecule that can increase AKT phosphorylation in mouse myocardium (Mak et al., 2010). Here we tested whether intraperitoneal (i.p.) administration of VO-OHpic could affect AKT/mTOR pathway also in the mouse brain. A single injection of VO-OHpic (i.p., 10 µg/kg) rapidly – 30 min post-injection - activated both AKT/mTOR and ERK1/2 signaling as well as the expression of components of the translational machinery in the forebrain. As shown in Figure 1A, VO-OHpic increased the expression of phospho-rpS6$^{Ser240-4}$ ($t_{(14)} = 5.45$, $p < 0.0001$), phospho-AKT ($t_{(8)} = 2.53$, $p = 0.035$), phospho-ERK ($t_{(8)} = 2.72$, $p = 0.027$) and EF1a ($t_{(13)} = 2.32$, $p = 0.037$), while it did not affect the levels of total rpS6 ($p = 0.07$), AKT ($p = 0.88$) and ERK ($p = 0.27$;vehicle, n=7; VO-OHpic, n = 8) proteins.

Because the activation of mTOR pathway is associated to the synthesis of brain-derived neurotrophic factor (BDNF) necessary for activity-dependent synaptic plasticity and memory formation (Inamura et al., 2005; Takei et al., 2001), we evaluated whether PTEN inhibition could trigger the expression of BDNF and the phosphorylation of its receptor, the tyrosine kinase TrkB (tropomyosin receptor kinase B). As shown in Figure 1B, no change was detected 30 min after VO-OHpic injection (BDNF: vehicle vs VO-OHpic $t_{(9)} = 1.93$, $p = 0.086$; pTrkB: vehicle vs VO-OHpic $t_{(9)} = 0.38$, $p = 0.72$ 0.05). Conversely, 6 h after VO-OHpic injection, there was a significant increase in BDNF levels (vehicle vs VO-OHpic $t_{(8)} = 2.51$; $p = 0.036$) and pTrkB (vehicle vs VO-OHpic $T_{(8)} = 3.5$; $p = 0.0081$). No change in total TrkB expression was observed at both time intervals (TrkB 30 min: $T_{(10)} = 0.66$, $p = 0.52$; 6 h: $T_{(16)} = 0.28$, $p = 0.78$; vehicle n=7; VO-OHpic n=8).

VO-OHpic injection affects dendritic spines turnover *in-vivo*

Previous studies showed that PTEN ablation modifies dendritic spines density (Skelton et al., 2019). Therefore, to investigated whether and how the inhibition of PTEN through VO-OHpic may interfere with spines organization, we turned to two-photon analysis in the somatosensory cortex (S1) of Thy1-GFP (M line) mice (Figure 1C) and assessed turnover dynamics. We found that a single injection of VO-OHpic influences spine turnover by reducing the short-term loss, but not the gain, of dendritic spines. As shown in Figure 1D-F, VO-OHpic significantly affected spine turnover ratio (vehicle: pre-injection vs. post-injection, $t_{(5)}= 0.78$, $p = 0.46$; VO-OHpic: pre-injection vs. post-injection, $t_{(5)}= 3.92$, $p = 0.011$) without affecting spine gain fraction (vehicle: pre-injection vs post-injection, $t_{(5)}= 1.40$, $p = 0.21$; VO-OHpic: pre-injection vs. post-injection, $t_{(5)}= 0.97$, $p = 0.37$) but reducing spine loss (vehicle: pre-injection vs. post-injection, $t_{(5)}= 0.15$, $p = 0.88$; VO-OHpic: pre-injection vs. post-injection, $t_{(5)}= 7.10$, $p = 0.0009$). Thus, these data show that VO-OHpic can alter dendritic spines dynamics in the cerebral cortex by reducing spine loss briefly after its injection.

VO-OHpic injection during memory consolidation enhances long- but not short-term memory

Our data showed that a single administration of VO-OHpic activates plasticity-relevant signaling pathways and modulated spine remodeling *in vivo*. We thus investigated if and how this compound may interfere with short- or long-term memory processes. To this aim, mice were trained to associate an acoustic stimulus (a pure tone of 1 kHz, acting as a conditioned stimulus, CS) to an aversive footshock (unconditioned stimulus, US). VO-OHpic or vehicle was administered immediately afterward to interfere specifically with the memory consolidation without affecting pain or sensory perception occurring during the acquisition trial (Sacchetti et al., 2002; Zhu et al. 2011; Cambiaghi et al., 2016). Animals were tested 1 h later to test VO-OHpic influence on short-term memory retention. Fear memory was tested by presenting the CSs in a totally new environment to avoid conditioned fear to contextual cues (Sacchetti et al., 2002; Zhu et al. 2011;

Cambiaghi et al., 2016). No differences were found between vehicle- and VO-OHpic-injected mice ($t_{(10)}$ = 0.05, p = 0.953; vehicle n = 6, VO-OHpic-injected n = 6 mice; Figure 2A). This data showed that VO-OHpic injection did not affect short-term memory and did not modify freezing behavior *per se*.

We then investigated the retention of long-term auditory memory by testing animals at 72 h, 2 and 4 weeks after learning (Figure 2B). In comparison to vehicle-injected mice, in VO-OHpic-injected mice long-term memory was significantly potentiated (2×3 mixed ANOVA, main effect of group $F_{(1, 16)}$ = 9.06, p = 0.008; main effect of time $F_{(2, 32)}$ = 2.78, p = 0.077; group×time interaction $F_{(2, 32)}$ = 1.77, p = 0.186) at 72 h (p = 0.003, vehicle, n=9, VO-OHpic, n=10 mice) and at 2 weeks (p = 0.021, vehicle n=9, VO-OHpic n=10), but not at 4 weeks, where there was only a tendency to memory potentiation (p = 0.173, vehicle n=8, VO-OHpic n=10; Figure 2B).

These results pose the question of whether the potentiation of long-term memory induced by VO-OHpic administration arises from a specific enhancement of memory processes or rather to an increment in fear-related processes. To address this, we analyzed the freezing elicited by the presentation of a tone (a 15 kHz-tone) never perceived before (Grosso et al., 2018; Concina et al., 2018, 2021, 2022). No differences were detected between the two groups ($t_{(10)}$ = 1.82, p = 0.098; n=6 mice for both groups; Figure 2C), thereby suggesting the absence of fear generalization in VO-OHpic-injected mice. These results revealed that the administration of VO-OHpic during memory consolidation improves the maintenance of long-term memory whereas it leaves unaffected short-term memory and fear generalization processes.

We next tested whether the administration of VO-OHpic may also improve contextual fear memory. Mice were therefore tested 48 h after learning. Surprisingly, the retention of contextual fear memory was left unchanged by PTEN inhibition ($t_{(10)}$ = 0.23, p = 0.822, n = 6 mice for both groups; Fig. 2D). We also performed an additional experiment by administering VO-OHpic (10 µM) directly into the dorsal hippocampus immediately after learning, and again we found no significant effects on long-term contextual memory ($t_{(6)}$ = 0.14, p = 0.889; vehicle, n = 4; VO-

OHpic, n = 4; Figure 2E, F). The latter result also supports the idea that VO-OHpic does not enhance basal fear. Combined, our results showed that the administration of VO-OHpic shortly after training elicited a selective long-term potentiation of auditory fear memory.

Changes in dendritic spines morphology underlie the enhancement of long-term auditory fear memory induced by VO-OHpic administration

We next sought to investigate which neural mechanisms triggered by VO-OHpic maintain potentiated fear memories over time. At first, we tested whether VO-OHpic administration was able to activate the mTOR pathway in the auditory cortex. We analyzed the posterior region of the auditory cortex, i.e: the secondary auditory cortex (Te2), because previous studies showed that this area plays an important role in the long-term maintenance of auditory fear memories (Sacco and Sacchetti, 2010; Grosso et al., 2015; Todd et al., 2018; Concina et al., 2019; 2022; Dalmay et al., 2019). Immunohistochemical analysis showed that 30 min after VO-OHpic injection, the density of neurons expressing p-rpS6$^{Ser240-4}$ in the Te2 cortex was robustly increased ($t_{(13)}$ = 2.35, p = 0.035, vehicle, n = 7; VO-OHpic, n = 8; Figure 3A,B). Because encoding of long-term memory is linked to a rearrangement of synaptic contacts and dendritic spines turnover in several brain regions (De Roo et al., 2008; Ruediger et al., 2011), including the auditory cortex (Moczulska et al., 2013; Yang et al., 2016), we assessed by DiOlistic labeling whether VO-OHpic can produce spines remodeling in layer 2/3 neurons of the Te2 region (Figure 3C-G). This analysis revealed that 6 hours after injection, VO-OHpic produced a significant increase in the density of immature spines compared to vehicle ($t_{(7)}$ = 2.93, p = 0.021, Figure 3F). In contrast, VO-OHpic produced no significant changes in the density of both mature dendritic spines ($t_{(7)}$ = 1.74, p = 0.12, Figure 3E) and total spine protrusions (total: $t_{(7)}$ = 0.82, p = 0.435; Figure 3D). Moreover, cumulative distribution of spines density based on neck/head ratio values (Figure 3G) revealed a rapid (6h after injection) rightward shift toward thin/long spines in VO-OHpic-treated animals compared to vehicle-treated controls (Kolmogorov-Smirnov- K-S: D= 0.143, p < 0.0001).

Next, we analyzed dendritic spine remodeling in layer 2/3 of Te2 at 72 h after training. Both density and morphology of dendritic spines were analyzed after DiOlistic labeling in the Te2 of conditioned or naïve mice injected with vehicle or VO-OHpic (Figure 3H-L). In vehicle-injected groups, the persistence of fear memories was associated with a significant increase of spines density in conditioned animals (n = 6) compared with naïve (n = 5) animals (two-way ANOVA, group $F_{(1,15)} = 15.88$, p = 0.001, followed by Fisher's LSD post hoc, conditioned-vehicle vs naive-vehicle, p = 0.011; Figure 3H,I). Similarly, in VO-OHpic-injected groups, conditioned mice (n = 4) showed a greater number of spines in comparison to naïve mice (n = 4; p = 0.013; Figure 3H,I). Moreover, the number of spines in naïve mice injected with VO-OHpic was similar to that of naïve mice that received the vehicle (p = 0.680). Thus, VO-OHpic by itself (i.e., in the absence of an associative learning process) did not elicit a persistent change in spine density. Surprisingly, there was no difference of spines density in conditioned mice that received the vehicle and in conditioned mice that received VO-OHpic (p= 0.430; Figure 3I). The latter result raises the question of if and how dendritic spine plasticity may be involved in the potentiation of long-term memory detected in VO-OHpic-injected conditioned mice. We therefore analyzed again mature or immature spines separately. Critically, no differences were detected among groups with regard to mature spines (two-way ANOVA, p = 0.094; Figure 3J), while there was a selective increase in the number of immature spines in conditioned mice injected with VO-OHpic with respect to those which received vehicle (two-way ANOVA, group $F_{(1,15)} = 15.73$, p = 0.001, followed by Fisher's LSD, p = 0.019; Figure 3K). VO-OHpic-injected conditioned mice also differed from naïve mice that received vehicle (p = 0.001) and naïve mice that received VO-OHpic (p = 0.001; Figure 3K). Interestingly, cumulative distribution of spines neck/head ratio shows a clear, although non-statistically significant (Kolmogorov-Smirnov- K-S: D = 0.105, p = 0.07; Figure 3L), rightward shift in VO-OHpic-treated conditioned animals compared to vehicle-treated conditioned mice, indicative of an higher density of filopodia-like protrusions. These data thus suggest that memory processes elicited an increase in the number of total dendritic spines in the auditory cortex. On the other hand, PTEN

inhibition potentiated long-term memory and this potentiation was associated with a persistent and selective increase of cortical immature spines.

Structural changes arise by the interplay between PTEN inhibition and memory processes

Thin-immature spines are transient highly plastic structures that are thought to maintain structural flexibility thus accommodating new, recently enhanced, or weakened inputs (Christoffel et al., 2011; Steffens et al., 2021). Our data suggest that this type of spine may be instrumental to maintain potentiated fear memory for a long time. To address this idea, we analyzed dendritic spines in the S1 cortex, an area not involved in long-term auditory fear memory. Firstly, we tested whether PTEN inhibition can activate in the S1 the phosphorylation of rpS6 at Ser 240-4 and spine growth. VO-OHpic injection produced an increase of $rpS6^{(Ser240-4)+}$ cells in all the layers of S1 30 min after its injection ($t_{(14)} = 2.92$, $p = 0.011$, vehicle, n = 7; VO-OHpic, n = 9; Figure 4A-B) and a subsequent (at 6 h) change in spine number in S1 ($t_{(6)} = 4.44$, $p = 0.004$, n = 4 in both groups; Figure 4C,D). Then, we analyzed spine morphology 6 hours after VO-Ohpic (or vehicle) injection also in S1 cortex (Figure 4C-G). Interestingly, spines morphology differed between vehicle and VO-OHpic-injected mice as VO-OHpic increased specifically the subpopulation of immature spines ($t_{(6)} = 2.69$, $p = 0.035$; Figure 4F) without affecting the mature spines ($t_{(6)} = 0.76$, $p = 0.471$; Figure 4E). Moreover, the rightward shift of neck/head ratios distribution curve indicates that VO-OHpic can rapidly (6h) induce an increase of thin/long dendritic spines also in S1 (Kolmogorov-Smirnov-K-S: $D = 0.173$, $p = 0.003$, Figure 4G). Finally, in the same conditioned mice where we detected changes in Te2 dendritic spines after learning, we analyzed dendritic spines in S1 cortex. No significant differences in total spines density were detected 72 hours after training in S1 of conditioned mice receiving vehicle (n = 4) or VO-OHpic (n = 4) compared to naïve animals (two-way ANOVA, $p = 0.429$; vehicle, n = 3; VO-OHpic, n = 4; Figure 4 H-L). Moreover, no differences

were detected between conditioned and naïve mice in the number of mature ($p = 0.322$; Figure 4J) and immature ($p = 0.234$; Figure 4K) spines. All these results are supported by the cumulative distribution data of neck/head ratio as assessed 72 hours after training in S1 (Kolmogorov-Smirnov-K-S: $D= 0.1$, $p = 0.516$; Figure 4L).

Hence, despite VO-OHpic being able to activate mTOR pathway and induce spine remodeling in S1 shortly after its injection, the persistence of immature spines did not occur at longer time intervals (i.e.: at 72 h after injection). These data suggest that the persistence of immature spine observed at long time intervals in Te2 of conditioned mice that received VO-OHpic arose specifically by the interplay between PTEN inhibition and long-term memory processes.

The blockade of mTORC1 activity prevents VO-OHpic-induced memory enhancement as well as structural changes in Te2

Finally, we assessed whether mTORC1 activity is necessary for long-lasting memory potentiation induced by VO-OHpic. At first, we investigated whether VO-OHpic action can be blocked by rapamycin, a selective inhibitor of mTORC1 (Belelovsky et al., 2009; Li et al., 2014;). Rapamycin injection abolished the phosphorylation of $rpS6^{Ser240-4}$ (two-way ANOVA, treatment $F_{(1,18)}= 5.99$, $p = 0.02$; vehicle+VO-OHpic vs rapamycin+VO-OHpic: $F_{(18)}= 2.69$, $p = 0.015$), which was similar to control animals (vehicle+vehicle vs rapamycin+VO-OHpic: $F_{(18)}= 0.39$, $p = 0.7$; Figure 5A,B). Rapamycin treatment produced also an effect on VO-OHpic-induced AKT phosphorylation (two-way ANOVA, interaction $F_{(1,18)}= 8.89$, $p = 0.008$; vehicle+VO-OHpic vs rapamycin+VO-OHpic: $F_{(18)}= 2.50$, $p = 0.022$) that was similar to vehicle-injected animals (vehicle+vehicle vs rapamycin+VO-OHpic: $F_{(18)}= 0.69$, $p > 0.09$; Figure 5A-C).

We then tested the effect of rapamycin on fear memory consolidation by injecting it after fear learning in vehicle- and VO-OHpic-injected mice. Rapamycin was administered 3 hours after learning because a previous study showed that rapamycin infused into the dorsal hippocampus

immediately or 180 min but not 540 min after training impairs long-term memory (Jobim et al., 2012). Rapamycin disrupted memory retention in both vehicle (n = 6) and VO-OHpic-injected (n = 6) mice at 72 h (vehicle-vehicle n = 5; VO-OHpic-vehicle, n = 6; two-way ANOVA, treatment $F_{(1,19)} = 105.05$, $p < 0.0001$; Figure 5D) and at 2 weeks (treatment $F_{(1,19)} = 101.0$, $p < 0.0001$; Figure 5E). Seventy-two hours after learning, in mice injected with VO-OHpic and rapamycin, freezing was lower with respect to VO-OHpic-vehicle injected animals ($p < 0.0001$), Interestingly, in VO-OHpic-rapamycin injected mice, freezing was higher than in animals injected with vehicle and rapamycin (VO-OHpic-rapamycin vs vehicle-rapamycin, $p = 0.020$; Figure 5D), thus suggesting the action of an alternative mechanism to mTORC1. Two weeks later, rapamycin disrupted memory recall in all groups (VO-OHpic-rapamycin vs VO-OHpic-vehicle, $p < 0.0001$; VO-OHpic-rapamycin vs vehicle-rapamycin, $p = 0.962$; Figure 5E). These results showed that mTORC inhibition affected long-term memory consolidation in control animals, and also hampered memory enhancement in VO-OHpic-injected mice.

We next investigated the effect of rapamycin administration on spines growth and remodeling associated with long-term fear memory (Figure 5F-J). In conditioned mice that received VO-OHpic and rapamycin (n = 3), the total spines density was lower with respect to conditioned animals that received VO-OHpic but not rapamycin (n = 4) (two-way ANOVA, group $F_{(2,19)} = 9.24$, $p = 0.001$ followed by Fisher's LSD, $p = 0.044$) while it was similar with respect to naïve mice that received VO-OHpic ($p = 0.559$; n = 4). In mice that did not receive VO-OHpic, rapamycin injection decreased the total spine density in conditioned mice (n = 3) at the level of naïve animals that did not receive rapamycin ($p = 0.263$; n = 5). While rapamycin globally left unaffected mature spines (two-way ANOVA, $p = 0.126$; Figure 5H), conditioned mice that received both VO-OHpic and rapamycin showed a lower number of immature spines with respect to conditioned animals that received VO-OHpic but not rapamycin (two-way ANOVA, group $F_{(2,19)} = 6.79$, $p = 0.005$ followed by Fisher's LSD, $p = 0.013$; Figure 5I). Finally, the cumulative distribution of neck/head ratios

showed that rapamycin prevented the appearance of thin/long spines as illustrated by the significant leftward shift of the frequency curves in both VO-OHpic- and vehicle-treated conditioned animals (vehicle-vehicle vs vehicle-rapamycin Kolmogorov-Smirnov - K-S: $D= 0.202$, $p < 0.001$; VO-OHpic-vehicle vs VO-OHpic-rapamycin Kolmogorov-Smirnov - K-S: $D= 0.215$, $p < 0.001$; Figure 5J). All these data show that mTORC1 activity is needed for the dynamic modifications of dendritic spines associated with memory obtained by PTEN inhibition.

DISCUSSION

Here we showed that the administration of VO-OHpic, a selective PTEN inhibitor, immediately after learning enhanced long- but not short-term auditory fear memories. This potentiation lasted several weeks and was associated with a long-lasting increase in immature dendritic spine numbers within the auditory cortex. Dendritic spines remodeling was specifically due to the interplay between VO-OHpic and memory processes, as it was absent in S1, a region not involved in auditory fear learning but where VO-OHpic induced spine growth shortly after its injection. Finally, rapamycin, a specific inhibitor of the mTORC1 complex, blocked both memory potentiation and immature spine growth.

In neurons, mTOR complex is present in the postsynaptic compartment, where it is triggered by activity and is critical for synaptic plasticity (Hoeffer and Klann, 2010; Switon et al., 2017). Most of this evidence comes from studies utilizing pharmacological or genetic inhibition of mTOR pathway. Here we applied a different approach. We investigated the possible effect of an enhancement of AKT/mTOR signaling pathway on dendritic spine remodeling and memory processes. We found that a single injection of VO-OHpic, the most selective and potent PTEN inhibitor (Rosivatz et al., 2006; Mak et al., 2010), rapidly activated AKT in the cerebral cortex and

6 hours after its injection it also increased spine density on layer 2/3 pyramidal cells in both S1 and Te2 areas. Critically, PTEN inhibition increased specifically the subpopulation of immature spines without affecting the density of mature spines. Indeed, two-photon in vivo imaging analysis of the effect of PTEN inhibition revealed a reduction of spine elimination on layer 5 pyramidal cells in S1. Although it is possible that spines turnover produced by VO-OHpic may not be equivalent in pyramidal cells from different layers (i.e.: 2/3 vs. 5), our data strongly suggest that PTEN inhibition acts critically on spine dynamics by stabilizing immature spines.

This study has some limitations. Somehow surprisingly, long-term memory enhancement was not associated with changes in spine morphology toward mature spines as suggested for memory storage mechanisms (Bourne and Harris, 2007). This can be due to factors involving the design of the current work and that shall be addressed in the future: specific morphological changes occurring in a subset of neurons, or spines, that become diluted (and not significant) in our sample; a different stability of immature spines produced by mechanism directly triggered by VO-OHpic enhanced memory; the timing (72h after training) of spine analyses or the treatment protocol (acute vs. chronic); the area of the auditory cortex in which we have focused our analysis (Te2 versus Te1). Previous works reported contrasting results: on one side, PTEN overexpression decreased spine density in the hippocampus while on the other, PTEN knockdown in the basolateral amygdala decreased total spine density inducing a shifting in the mushroom/thin ratio with an increase of mushroom spines (Haws et al., 2014). In line with our findings, a previous study demonstrated that a peptide which activates the PI3K signaling pathway induced the formation of small, “thin” spines in both hippocampus and cell culture (Enriquez-Barreto et al., 2014). Notably, our results also showed that in the absence of associative processes the increase in immature spines induced by PTEN inhibition is a transient process disappearing 72 hours after VO-OHpic injection. In contrast, spine remodeling becomes more persistent when it is linked to memory processes and, in this condition, it may enhance long-term memories. Thus, independently from the mechanism of action,

these data underscore the importance of the mTOR pathway as a potential druggable target for enhancing learning and memory.

We administered VO-OHpic after learning, and memory retention was tested several days later so that it would act specifically on memory consolidation processes, without interfering either with acquisition or retrieval phases. This allows excluding state-dependent effects and interference with CS and US perception and motor functions (Sacchetti et al., 2002; Cambiaghi et al., 2016). By doing this, we found a selective potentiation of auditory fear memories. In contrast to our findings, a previous study showed that VO-OHpic infusion over a period of 3–4 weeks into brain ventricles did not affect auditory fear memory (Knafo et al., 2016). Despite differences in the type and timing of VO-OHpic administration (a single injection immediately after learning vs. prolonged infusion before learning) might account for this discrepancy, future studies should further address this point. In the same study (Knafo et al., 2016), the prolonged VO-OHpic administration did not modify the retention of long-term contextual fear memory while it rescued normal hippocampal synaptic function and memory dysfunctions in animal models of Alzheimer's disease. Together with our findings, also showing a lack of effects of a single intrahippocampal injection of VO-OHpic on the long-term long-term contextual fear memory, these data suggest that PTEN modulation may counteract hippocampal synaptic dysfunction and cognitive deficits but not enhance hippocampal-dependent memories in physiological conditions.

Long-term memory potentiation induced by VO-OHpic was accompanied by a selective increment in the number of immature spines in the more posterior region of the auditory cortex, the Te2 cortex, that plays a crucial role in long-term auditory fear memories (Sacco and Sacchetti, 2010; Grosso et al., 2015; Todd et al., 2018; Concina et al., 2019,2022; Dalmay et al., 2019). In contrast, although 6 hours after its injection VO-OHpic produced an increase of immature spines also in S1, an area unrelated to memory consolidation,this increment was no longer present at 72 hours in the same animals where spines growth occurred in Te2. We propose that PTEN inhibition and the consequent increase in mTORC activity elicit morphological changes at the level of

dendritic spines. When interacting with memory processes, this determines a persistent increase in immature spines and the strength of enduring memories. The morphology of dendritic spines is a factor influencing spine stability and function and long-lasting changes in synaptic activity are accompanied by alterations in spine shape, size, and number (Hering and Sheng, 2001; Gipson and Olive, 2017; Pchitskaya and Bezprozvanny, 2020). Thin-immature spines are highly plastic structures that respond to synaptic activity underlying learning processes (Gipson and Olive, 2017). These protrusions maintain structural flexibility to enlarge and stabilize (or shrink and dismantle), as they accommodate new inputs (Bourne and Harris, 2007; Lu and Zuo, 2017). Moreover, smaller spines preferentially undergo long-term potentiation, whereas larger spines are more stable and show less plasticity. Such observations led to the idea that thin-immature spines represent "plasticity" or "learning" spines (Bourne and Harris, 2007; Huang et al., 2020). In this framework, our study showed that a potentiation of long-term memory over time is associated with a persistent increase of immature spines.

mTOR exists in two distinct complexes, mTORC1 and mTORC2 (Kim et al., 2002; McCabe et al., 2020), both of them can be involved in memory processes (Kim et al., 2002; Costa-Mattioli et al., 2009; Huang et al., 2020; McCabe et al., 2020). Here we found that memory potentiation produced by VO-OHpic requires mTORC1. VO-OHpic was administered immediately after training allowing the activation of mTOR and BDNF signaling, the latter activating protein translation at dendrites through an mTOR-dependent pathway (Takei et al., 2004). Rapamycin blocked mTORC1 activity 3 hours later, probably affecting the second-wave of S6K1 phosphorylation (Garelick et al., 2013; Tee, 2018). In the presence of rapamycin, VO-OHpic-injected mice performed significantly better than vehicle-injected animals at 72 hours after learning, thereby suggesting the action of alternative rapamycin-insensitive mechanism(s). However, our data suggest that this mechanism alone, i.e.: in the absence of mTORC1 activity, is not sufficient to maintain memory strengthening at more distant time intervals.

In conclusion, our study provides new insights into the molecular mechanisms underlying the maintenance of long-term memories and on the cellular processes that may aid enhancing them. Treatments aimed at counteracting age-related cognitive decline result in an increase in the number of thin spines, suggesting that thin spines are necessary to restore the potential for synaptic plasticity in the aged brain and memory-related diseases (Morrison and Baxter, 2012). Because our study addressed structural modifications in relatively young animals (i.e.: 8-9 weeks of age), it will be of paramount interest to investigate in the future whether the modulation of PTEN activity can promote long-term memory enhancement also in older animals, as dendritic spines dynamics in the cerebral cortex profoundly change with aging (Davidson et al., 2020). Moreover, recent studies showed that in schizophrenia patients small spine density is significantly reduced in primary and secondary cortical regions and this may contribute to auditory deficits (Parker and Sweet, 2018). Indeed, individuals with schizophrenia demonstrate auditory hallucinations and deficits in both auditory stimuli processing and auditory memory, which contribute to socio-cognitive dysfunction (Javitt and Sweet, 2015; Kantrowitz et al., 2016, Parker and Sweet, 2018). In this framework, our findings may provide new insights for a novel approach aimed at counteracting small spine reductions and auditory memory dysfunction in schizophrenia.

References

Amendola E, Zhan Y, Mattucci C, Castroflorio E, Calcagno E, Fuchs C, Lonetti G, Silingardi D, Vyssotski AL, Farley D, Ciani E, Pizzorusso T, Giustetto M, Gross CT (2014) Mapping pathological phenotypes in a mouse model of CDKL5 disorder. PLoS One 9,e91613.

Belelovsky K, Kaphzan H, Elkobi A, Rosenblum K (2009) Biphasic activation of the mTOR pathway in the gustatory cortex is correlated with and necessary for taste learning. J Neurosci 29:7424-7431.

Bohlen J, Roiuk M, Teleman AA (2021) Phosphorylation of ribosomal protein S6 differentially affects mRNA translation based on ORF length. Nucleic Acids Research 49:13062-13074.

Bourne J, Harris KM. (2007) Do thin spines learn to be mushroom spines that remember? Current Opinion in Neurobiology 17: 381-386.

Cambiaghi M, Grosso A, Renna A, Sacchetti B (2016) Differential Recruitment of Auditory Cortices in the Consolidation of Recent Auditory Fearful Memories. J Neurosci 36: 8586-8597.

Chapleau CA, Boggio EM, Calfa G, Percy AK, Giustetto M, Pozzo-Miller L (2012) Hippocampal CA1 pyramidal neurons of Mecp2 mutant mice show a dendritic spine phenotype only in the presymptomatic stage. Neural Plasticity 2012*:* 976164.

Christoffel DJ, Golden SA, Russo SJ (2011) Structural and synaptic plasticity in stress-related disorders. Reviews in Neuroscience 22: 535-549.

Ciccarelli A, Calza A, Santoru F, Grasso F, Concas A, Sassoè-Pognetto M, Giustetto M (2013) Morphine withdrawal produces ERK-dependent and ERK-independent epigenetic marks in neurons of the nucleus accumbens and lateral septum. Neuropharmacology 70:168-79.

Concina G, Cambiaghi M, Renna A, Sacchetti B (2018) Coherent Activity between the Prelimbic and Auditory Cortex in the Slow-Gamma Band Underlies Fear Discrimination. J Neurosci 38: 8313-8328.

657 Concina G, Renna A, Grosso A, Sacchetti B (2019) The auditory cortex and the emotional valence
658 of sounds. Neuroscience Biobehavioral Reviews 98: 256-264.

659 Concina G, Renna A, Grosso A, Sacchetti B (2022) Prior fear learning enables the rapid
660 assimilation of new fear memories directly into cortical networks. Plos Biology 20:e3001789.

661 Concina G, Renna A, Milano L, Manassero E, Stabile F, Sacchetti B (2021) Expression of IGF-2
662 Receptor in the Auditory Cortex Improves the Precision of Recent Fear Memories and Maintains
663 Detailed Remote Fear Memories Over Time. Cerebral Cortex 31: 5381-5395.

664 Costa-Mattioli M, Sossin WS, Klann E, Sonenberg N (2009) Translational control of long-lasting
665 synaptic plasticity and memory. Neuron 61: 10-26.

666 Dalmay T, Abs E, Poorthuis RB, Hartung J, Pu DL, Onasch S, Lozano YR, Signoret-Genest J,
667 Tovote P, Gjorgjieva J, Letzkus JJ (2019) A Critical Role for Neocortical Processing of Threat
668 Memory. Neuron 104: 1180-1194.e7.

669 Davidson AM, Mejía-Gómez H, Jacobowitz M, Mostany R (2020) Dendritic Spine Density and
670 Dynamics of Layer 5 Pyramidal Neurons of the Primary Motor Cortex Are Elevated With Aging.
671 Cereb Cortex 30:767-777.

672 Della Sala G, Putignano E, Chelini G, Melani R, Calcagno E, Michele Ratto G, Amendola E, Gross
673 CT, Giustetto M, Pizzorusso T (2016) Dendritic Spine Instability in a Mouse Model of CDKL5
674 Disorder Is Rescued by Insulin-like Growth Factor 1. Biological Psychiatry 80: 302-311.

675 De Roo M, Klauser P, Garcia PM, Poglia L, Muller D (2008) Spine dynamics and synapse
676 remodeling during LTP and memory processes. Progress in Brain Research 169: 199-207.

677 Enriquez-Barreto L, Cuesto G, Dominguez-Iturza N, Gavilán E, Ruano D, Sandi C, Fernández-Ruiz
678 A, Martín-Vázquez G, Herreras O, Morales M (2014) Learning improvement after PI3K activation
679 correlates with de novo formation of functional small spines. Frontiers in Molecular Neuroscience
680 2: 6-54.

681 Garelick MG, Mackay VL, Yanagida A, Academia EC, Schreiber KH, Ladiges WC, Kennedy BK
682 (2013) Chronic rapamycin treatment or lack of S6K1 does not reduce ribosome activity in vivo.
683 Cell Cycle 12: 2493-2504.

684 Garza-Lombó C, Gonsebatt ME (2016) Mammalian Target of Rapamycin: Its Role in Early Neural
685 Development and in Adult and Aged Brain Function. Frontiers in Cellular Neuroscience 10:157.

686 Gipson CD, Olive MF (2017) Structural and functional plasticity of dendritic spines - root or result
687 of behavior? Genes Brain and Behavior 16: 101-117.

688 Graber TE, McCamphill PK, Sossin WS (2013) A recollection of mTOR signaling in learning and
689 memory. Learning and Memory 20: 518-530.

690 Grosso A, Cambiaghi M, Renna A, Milano L, Merlo RG, Sacco T, Sacchetti B (2015) The higher
691 order auditory cortex is involved in the assignment of affective value to sensory stimuli. Nature
692 Communications 6-8886.

693 Grosso A, Santoni G, Manassero E, Renna A, Sacchetti B (2018) A neuronal basis for fear
694 discrimination in the lateral amygdala. Nature Communications 9: 1214.

695 Hay N, Sonenberg N (2004) Upstream and downstream of mTOR. Genes and Development 18:
696 1926-1945.

697 Haws ME, Jaramillo TC, Espinosa F, Widman AJ, Stuber GD, Sparta DR, Tye KM, Russo SJ,
698 Parada LF, Stavarache M, Kaplitt M, Bonci A, Powell CM (2014) PTEN knockdown alters
699 dendritic spine/protrusion morphology, not density. Journal of Comparative Neurology 522: 1171-
700 1190.

701 Hering H, Sheng M (2001) Dendritic spines: structure, dynamics and regulation. Nature Reviews
702 Neuroscience 2: 80-88.

703 Hoeffer CA, Klann E (2010) mTOR signaling: at the crossroads of plasticity, memory and disease.
704 Trends in Neuroscience 33: 67-75.

705 Huang L, Zhou H, Chen K, Chen X, Yang G (2020) Learning-dependent dendritic spine plasticity is
706 reduced in the aged mouse cortex. Frontiers in Neural Circuits 26: 14:581435

707 Huang W, Zhu PJ, Zhang S, Zhou H, Stoica L, Galiano M, Krnjević K, Roman G, Costa-Mattioli M
708 (2013) mTORC2 controls actin polymerization required for consolidation of long-term memory.
709 Nat Neuroscience 16: 441-448.

710 Inamura N, Nawa H, Takei N (2005) Enhancement of translation elongation in neurons by brain-
711 derived neurotrophic factor: implications for mammalian target of rapamycin signaling. Journal of
712 Neurochemistry 95: 1438–1445.

713 Iwanami A, Cloughesy TF, Mischel PS (2009) Striking the balance between PTEN and PDK1: it all
714 depends on the cell context. Genes and Development 23:1699-704.

715 Jacinto E, Facchinetti V, Liu D, Soto N, Wei S, Jung SY, Huang Q, Qin J, Su B (2006) SIN1/MIP1
716 maintains rictor-mTOR complex integrity and regulates Akt phosphorylation and substrate
717 specificity. Cell 127: 125-137.

718 Javitt DC, Sweet RA (2015) Auditory dysfunction in schizophrenia: integrating clinical and basic
719 features. Nat Rev Neurosci 16: 535-50.

720 Jobim PF, Pedroso TR, Werenicz A, Christoff RR, Maurmann N, Reolon GK, Schröder N, Roesler
721 R (2012) Impairment of object recognition memory by rapamycin inhibition of mTOR in the
722 amygdala or hippocampus around the time of learning or reactivation. Behavioral Brain Research
723 228:151-158.

724 Kantrowitz JT, Epstein ML, Beggel O, Rohrig S, Lehrfeld JM, Revheim N, Lehrfeld NP, Reep J,
725 Parker E, Silipo G, Ahissar M, Javitt DC (2016) Neurophysiological mechanisms of cortical
726 plasticity impairments in schizophrenia and modulation by the NMDA receptor agonist D-serine.
727 Brain. 139:3281-3295.

728 Kim DH, Sarbassov DD, Ali SM, King JE, Latek RR, Erdjument-Bromage H, Tempst P, Sabatini
729 DM (2002) mTOR interacts with raptor to form a nutrient-sensitive complex that signals to the cell
730 growth machinery. Cell 110: 163–175.

731 Knafo S et al. (2016) PTEN recruitment controls synaptic and cognitive function in Alzheimer's
732 models. Nat Neuroscience 19: 443-53.

733 Koehl M, Ladevèze E, Catania C, Cota D, Abrous DN (2021) Inhibition of mTOR signaling by
734 genetic removal of p70 S6 kinase 1 increases anxiety-like behavior in mice. Translational
735 Psychiatry 11: 65.

736 Landi S, Putignano E, Boggio EM, Giustetto M, Pizzorusso T, Ratto GM (2011) The short-time
737 structural plasticity of dendritic spines is altered in a model of Rett syndrome. Scientific Report 1-
738 45.

739 Li J, Kim SG, Blenis J (2014) Rapamycin: one drug, many effects. Cell Metabolism 19: 373-379.

740 Lu J, Zuo Y (2017) Clustered structural and functional plasticity of dendritic spines. Brain Res Bull
741 129: 18-22.

742 Mac Callum PE, Hebert M, Adamec RE, Blundell J (2014) Systemic inhibition of mTOR kinase via
743 rapamycin disrupts consolidation and reconsolidation of auditory fear memory. Neurobiology of
744 Learning and Memory 112: 176-185.

745 McCabe MP, Cullen ER, Barrows CM, Shore AN, Tooke KI, Laprade KA, Stafford JM, Weston
746 MC (2020) Genetic inactivation of mTORC1 or mTORC2 in neurons reveals distinct functions in
747 glutamatergic synaptic transmission. Elife 3: 9:e51440.

748 Mak LH, Vilar R, Woscholski R (2010) Characterisation of the PTEN inhibitor VO-OHpic. Journal
749 of Chemical Biology 3: 157-163.

750 Meziane H, Khelfaoui M, Morello N, Hiba B, Calcagno E, Reibel-Foisset S, Selloum M, Chelly J,
751 Humeau Y, Riet F, Zanni G, Herault Y, Bienvenu T, Giustetto M, Billuart P (2016) Fasudil
752 treatment in adult reverses behavioural changes and brain ventricular enlargement in Oligophrenin-
753 1 mouse model of intellectual disability. Human Molecular Genetics 25:2314-2323.

754 Moczulska KE, Tinter-Thiede J, Peter M, Ushakova L, Wernle T, Bathellier B, Rumpel S (2013)
755 Dynamics of dendritic spines in the mouse auditory cortex during memory formation and memory
756 recall. Proc Natl Acad Sci U S A 110: 18315-18320.

757 Morrison JH, Baxter MG (2012) The ageing cortical synapse: hallmarks and implications for
758 cognitive decline. Nat Rev Neurosci 13:240-250.

759 Parker EM, Sweet RA (2018) Stereological Assessments of Neuronal Pathology in Auditory Cortex
760 in Schizophrenia. Front Neuroanat 9:11:131

761 Paxinos G, Watson C (2007) The Rat Brain in Stereotaxic Coordinates. *Academic Press Elsevier*,
762 London.

763 Pchitskaya E, Bezprozvanny I (2020) Dendritic Spines Shape Analysis-Classification or
764 Clusterization? Perspective. Frontiers in Synaptic Neuroscience 12:31.

765 Pizzo R, Gurgone A, Castroflorio E, Amendola E, Gross C, Sassoè-Pognetto M, Giustetto M (2016)
766 Lack of Cdkl5 disrupts the organization of excitatory and inhibitory synapses and parvalbumin
767 interneurons in the primary visual cortex. Frontiers in Cellular Neuroscience 10: 261

768 Rosivatz E, Matthews JG, McDonald NQ, Mulet X, Ho KK, Lossi N, Schmid AC, Mirabelli M,
769 Pomeranz KM, Erneux C, Lam EW, Vilar R, Woscholski R (2006) A small molecule inhibitor for
770 phosphatase and tensin homologue deleted on chromosome 10 (PTEN). *ACS* Chemical Biology 1:
771 780-790.

772 Roux PP, Topisirovic I (2018) Signaling Pathways Involved in the Regulation of mRNA
773 Translation. Molecular Cell Biology 38e00070-18.

774 Ruediger S, Vittori C, Bednarek E, Genoud C, Strata P, Sacchetti B, Caroni P (2011) Learning-
775 related feedforward inhibitory connectivity growth required for memory precision. Nature 473: 514-
776 518.

777 Sacchetti B, Baldi E, Lorenzini CA, Bucherelli C (2002) Cerebellar role in fear-conditioning
778 consolidation. Proc Natl Acad Sci U S A 99: 8406-8411.

779 Sacchetti B, Lorenzini CA, Baldi E, Tassoni G, Bucherelli C (1999) Auditory thalamus, dorsal
780 hippocampus, basolateral amygdala, and perirhinal cortex role in the consolidation of conditioned
781 freezing to context and to acoustic conditioned stimulus in the rat. J Neurosci 19: 9570-9578.

782 Sacco T, Sacchetti B (2010) Role of secondary sensory cortices in emotional memory storage and
783 retrieval in rats. Science 329: 649-56.

784 Saxton RA, Sabatini DM (2017) mTOR Signaling in Growth, Metabolism, and Disease. Cell 68:
785 960-976.

786 Shiota C, Woo JT, Lindner J, Shelton KD, Magnuson MA (2006) Multiallelic disruption of the
787 rictor gene in mice reveals that mTOR complex 2 is essential for fetal growth and viability.
788 Developmental Cell 11: 583-589.

789 Skelton PD, Frazel PW, Lee D, Suh H, Luikart BW (2019) Pten loss results in inappropriate
790 excitatory connectivity. Molecular Psychiatry 24: 1627-1640.

791 Steffens H, Mott AC, Li S, Wegner W, Švehla P, Kan VWY, Wolf F, Liebscher S, Willig KI (2021)
792 Stable but not rigid: Chronic in vivo STED nanoscopy reveals extensive remodeling of spines,
793 indicating multiple drivers of plasticity. Science Advances 7.

794 Sun J, Liu Y, Tran J, O'Neal P, Baudry M, Bi X (2016) mTORC1-S6K1 inhibition or mTORC2
795 activation improves hippocampal synaptic plasticity and learning in Angelman syndrome mice.
796 Cellular Molecular Life Science 3:4303-4314.

797 Switon K, Kotulska K, Janusz-Kaminska A, Zmorzynska J, Jaworski J (2017) Molecular
798 neurobiology of mTOR. Neuroscience 341: 112-153.

799 Takei N, Inamura N, Kawamura M, Namba H, Hara K, Yonezawa K, Nawa H (2004) Brain-derived
800 neurotrophic factor induces mammalian target of rapamycin-dependent local activation of
801 translation machinery and protein synthesis in neuronal dendrites. J Neurosci 24: 9760-9769.

802 Takei N, Kawamura M, Hara K, Yonezawa K, Nawa H (2001) Brain-derived neurotrophic factor
803 enhances neuronal translation by activating multiple initiation processes: comparison with the
804 effects of insulin. Journal of Biological Chemistry 276: 42818–42825.

805 Tee AR (2018) The Target of Rapamycin and Mechanisms of Cell Growth. International Journal of
806 Molecular Sciences 19: 880.

807 Todd TP, Jiang MY, DeAngeli NE, Bucci DJ (2018) A functional circuit for the retrieval of remote
808 cued fear memory. Behavioral Neuroscience 132: 403-408.

809 Yang Y, Liu DQ, Huang W, Deng J, Sun Y, Zuo Y, Poo MM (2016) Selective synaptic remodeling
810 of amygdalocortical connections associated with fear memory. Nat Neuroscience 19: 1348-1355.

811 Zhou H, Huang S (2010) The complexes of mammalian target of rapamycin. Current Protein and
812 Peptide Science 11: 409-424.

813 Zhu PJ, Chen CJ, Mays J, Stoica L, Costa-Mattioli M (2018) mTORC2, but not mTORC1, is
814 required for hippocampal mGluR-LTD and associated behaviors. Nat Neuroscience 21:799-802.

815 Zhu L, Sacco T, Strata P, Sacchetti B (2011) Basolateral amygdala inactivation impairs learning-
816 induced long-term potentiation in the cerebellar cortex. PLoS One. 31: 6:e16673.

817

Figure Legends

Figure 1. PTEN inhibition with a single injection of VO-OHpic activates AKT/mTOR pathway and affects dendritic spines turnover. **A**, Representative western blots of PI3K/AKT/mTOR pathway proteins. Quantitative analysis shows that AKT (Ser473), ERK (Thr 202/Tyr204) and rpS6(SER240-4) phosphorylation as well as EF1α expression significantly increased in mouse forebrain 30' after VO-OHpic injection. Vinculin was used as loading control. **B**, Representative western blots of BDNF and pTrkB. Optical density analysis shows that both BDNF and pTrkB expression was unchanged 30' after VO-OHpic treatment but almost doubled 6 hours later. Actin was used as loading control. **C**, Two-photon imaging experimental design. **D**, Images of a dendritic branch from VO-OHpic and vehicle-treated mice before and after the injection. Asterisks indicate lost spines that were lost while arrowheads point to gained spines through this period. **E-F**, VO-OHpic significantly affected spine turnover ratio. PTEN inhibition prevented the loss of immature spines compared (**F**) to vehicle-treated mice (**E**). Data are expressed as mean ± SEM. Student t-test: * $p<0.05$; ** $p<0.01$; ***$p<0.001$). Scale bar = 5 µm.

Figure 2. The administration of VO-OHpic during memory consolidation enhances long- but not short-term memory. **A**, VO-OHpic did not affect short-term memory compared to mice receiving vehicle 1 h after conditioning. **B**, Conversely, it significantly increased long-lasting memory at 72 h and 2 weeks, but not at 4 weeks. **C**, No differences were found between mice receiving vehicle or VO-OHpic during the presentation of a new tone 72 h after conditioning. **D**, Vehicle and VO-OHpic-injected mice did not differ from each other in the contextual freezing 48 h after learning. **E-F**, Bilateral intra-hippocampal infusion of 10 µM VO-OHpic did not affect long-term contextual memory. In the left panel, the arrow indicates a track needle in the dorsal hippocampus. Student t-test and 2×3 mixed ANOVA: *$p < 0.05$, **$p < 0.01$. Data are expressed as mean ± SEM.

Figure 3. Memory potentiation induced by VO-OHpic injection correlates with a long-term increment of immature dendritic spines in the auditory cortex. **A,** Representative micrographs of Te2 cryosections showing the effect of PTEN inhibition on p-rpS6 (Ser240/244) immunoreactivity 30' after VO-OHpic injection. Scale bar = 100 µm. **B**, Bar graphs illustrate $rpS6^{240+}$ cell density 30' after VO-OHpic injection. **C,** Representative images in Te2 of L2/3 pyramidal neuron dendrites from vehicle- or VO-OHpic-injected mice stained with DiOlistic. Scale bar = 5 µm; arrows: immature spines; arrowheads mature spines. **D-F**, Total spine density remained unchanged in both vehicle and VO-OHpic conditions. No significant difference was detected in mature spine density (**E**), while immature spines increased after VO-OHpic injection (**F**). **G**, Cumulative analysis of spines distribution based on neck/head ratio; dotted line: immature/mature spines cut-off point. **H**, Representative images of Te2 pyramidal neurons dendrites in naïve and conditioned mice. Scale bar = 5 µm. **I-K**, Total dendritic spine density was increased 72 h after training in both vehicle- and VO-OHpic- injected mice compared with naive animals. Mature spines density remained unchanged after VO-OHpic injection (**J**) while immature spines were significantly increased (**K**). **L**, Cumulative analysis of spines neck/head ratio; dotted line: immature/mature spines cut-off point. Student t-test, two-way ANOVA and Fisher's LSD post hoc test and Kolmogorov–Smirnov (KS) fitting test; $*p < 0.05$, $**p < 0.01$, $***p < 0.001$. Data are expressed as mean ± SEM.

Figure 4 VO-OHpic effects on dendritic spines morphology in the primary somatosensory cortex. **A,** Representative micrographs of S1 cryosections showing the effect of PTEN inhibition on p-rpS6 (Ser240/244) immunoreactivity 30' after VO-OHpic injection. Scale bar = 100 µm. **B,** Bar graphs illustrate $rpS6^{240+}$ cell density increase in S1 of treated animals. **C**, Representative images of pyramidal neuron dendrites in S1 from vehicle- or VO-OHpic-injected mice stained with DiOlistic. Scale bar = 5 µm. **D-F**, Bar graphs showing that 6 h after PTEN inhibition the density of both total (**D**) and immature spines was significantly increased (**F**), while mature spines remained unaffected

(**E**). **G**, Cumulative analysis of spines neck/head ratio; dotted line: immature/mature spines cut-off point. **H**, Representative S1 cortical dendrites stained with DiOlistic. Scale bar = 5 µm. **I-K**, No significant differences in spines density and morphology were detected 72 h after training. **L,** Cumulative analysis of spines neck/head ratio; dotted line: immature/mature spines cut-off point. Student t-test, two-way ANOVA and Fisher's LSD post hoc test; Kolmogorov–Smirnov (KS) fitting test; *p < 0.05, **p < 0.01, ***p < 0.001. Data are expressed as mean ± SEM.

Figure 5. Rapamycin impairs both long-term memory retention and VO-OHpic-induced memory enhancement as well as changes of spines structure. **A**, Representative western blot of forebrain lysates of mice receiving rapamycin (4.5 mg/kg i.p.) or vehicle 3h before PTEN inhibition. **B-C**, Western blot quantifications revealed that rapamycin blocked VO-OHpic-induced phosphorylation of rpS6 (Ser240-4) but did not affect pAKT (Ser473) expression. Vinculin was used as loading control. **D**, Rapamycin disrupted memory retention in both vehicle and VO-OHpic-injected mice at 72 h after learning. **E**, Two weeks later, rapamycin severely disrupted memory recall in both groups. **F**, Representative images of pyramidal neuron dendrites stained with Diolistic in Te2 from mice that received either vehicle- or VO-OHpic (left) and rapamycin (right) 72 h after training. **G**, Bar graphs showing that rapamycin significantly affected the increase of total number of spines only in VO-OHpic-injected conditioned animals. Rapamycin specifically impaired the growth of immature spines (**I**) and left mature spines density unaffected (**H**). **J**, Cumulative distribution of spines neck/head ratio; dotted line: immature/mature spines cut-off point. Scale bar = 5 µm. Two-way ANOVA and Fisher's LSD post hoc and Kolmogorov–Smirnov (KS) fitting test; *p < 0.05, **p < 0.01, ***p < 0.001. Data are expressed as mean ± SEM.

Figure1

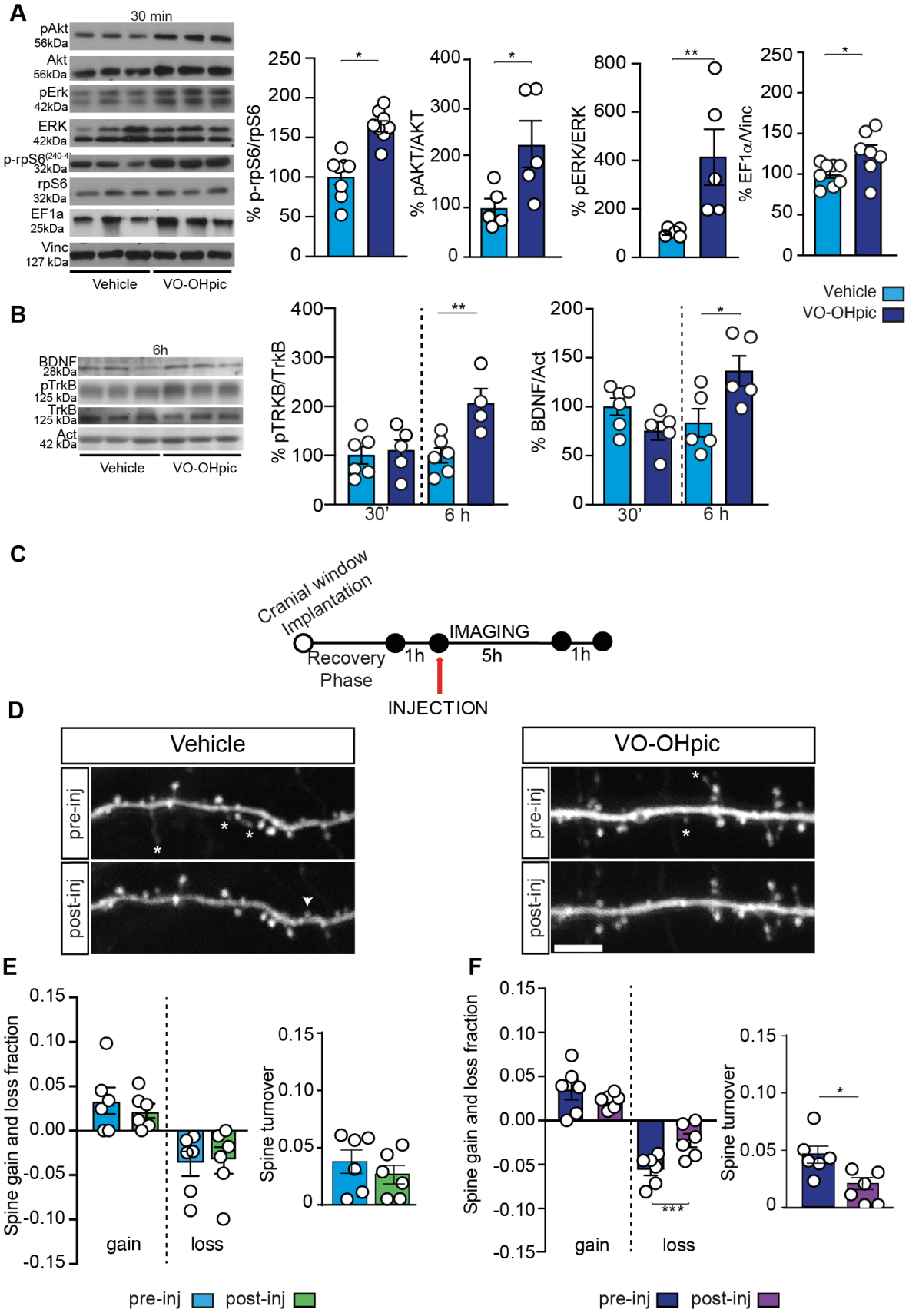

Figure 2

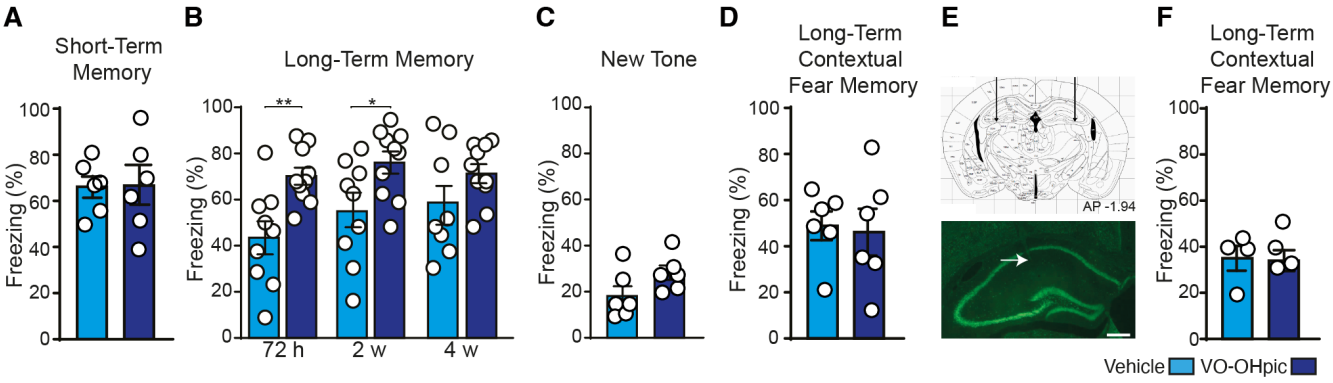

Figure 3

Te2 cortex

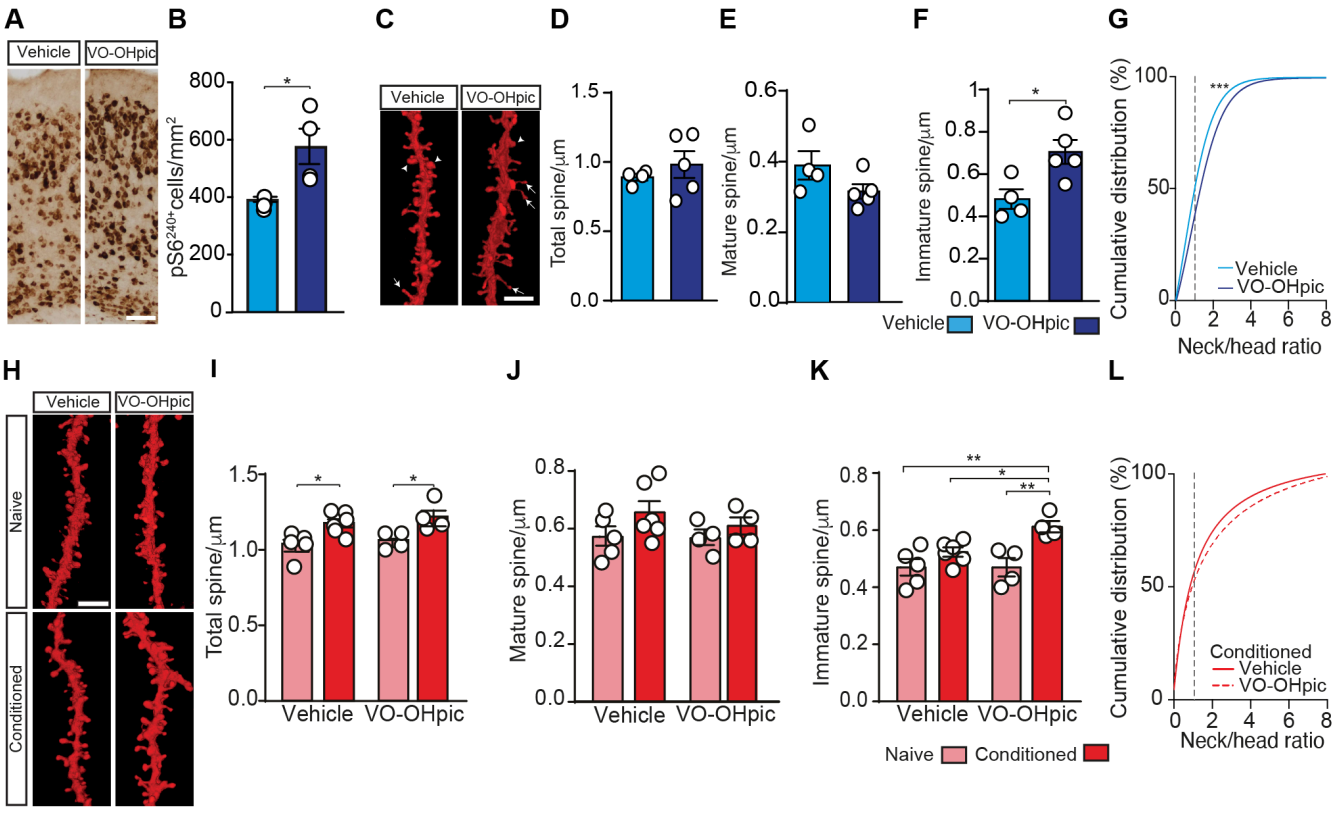

Figure 4

S1 cortex

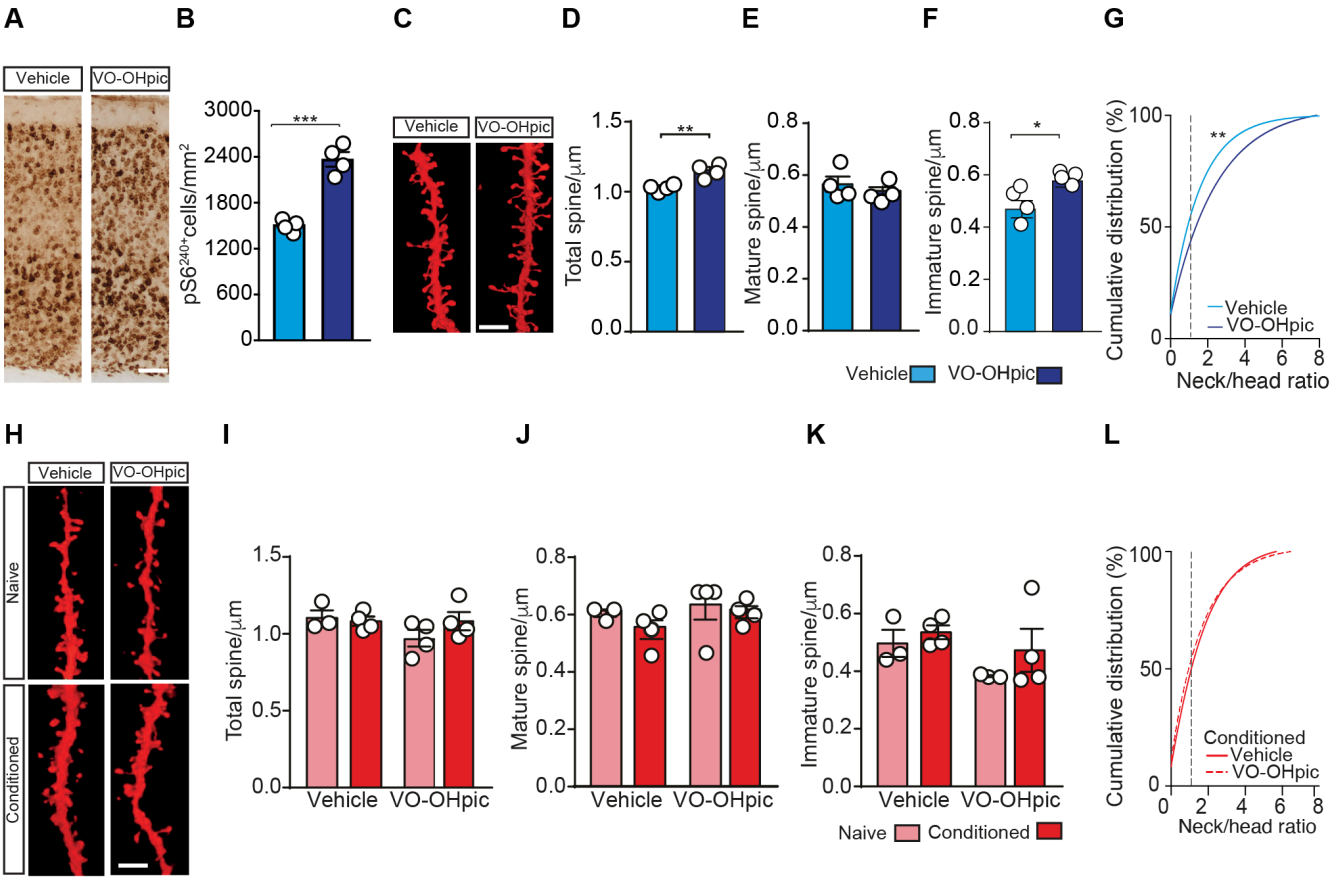

Figure 5